NASA

Technical Memorandum 82147

Multiple Crossings of a Very Thin Plasma Sheet in the Earth's Magnetotail

D.H. Fairfield, E.W. Hones,Jr., C.-I. Meng

JUNE 1981

National Aeronautics and Space Administration

Goddard Space Flight Center
Greenbelt, Maryland 20771

MULTIPLE CROSSINGS OF A VERY THIN PLASMA SHEET IN THE EARTH'S MAGNETOTAIL

D. H. Fairfield
Laboratory for Extraterrestrial Physics
NASA/Goddard Space Flight Center
Greenbelt, Maryland 20771

E. W. Hones, Jr.
Los Alamos Scientific Laboratory
University of California
Los Alamos, New Mexico 87545

C.-I. Meng
Applied Physics Laboratory
The Johns Hopkins University
Laurel, Maryland 20810

ABSTRACT

High resolution magnetic field, plasma and energetic particle data from the IMP-8 spacecraft have been used to study multiple crossings of the earth's magnetotail plasma sheet when it becomes thin during magnetospheric substorms. IMP-8 is found to traverse the entire thickness of the $\beta > 1$ plasma sheet in times that are as short as 10 s. Such traversals recur on a time scale of several minutes and they are associated with high velocity plasma flows that are usually directed tailward but are occasionally directed earthward for brief intervals. We argue that these observations can be explained by rapid oscillations of a plasma sheet that is only a few thousand kilometers thick, a dimension that is comparable to the gyroradius of energetic protons. When protons of 50 keV and 290 keV are detected at a location on tail lobe field lines near the plasma sheet, they are often seen to be moving in the dawn to dusk direction and may be undergoing serpentine cross tail motion. Differences in the angular distributions of the two energies indicate that the higher energy protons are preferentially located on field lines deeper in the tail lobe. This result is consistent with proton acceleration at a neutral line with subsequent $\vec{E}x\vec{B}$ drift in a cross-tail electric field that moves the lower energy particles closer to the equatorial plane. A neutral line acceleration model is also supported by our observation that tailward streaming energetic electrons are occasionally present at the lobe-plasma sheet interface.

INTRODUCTION

The plasma sheet in the earth's magnetotail has an average thickness of about 4-6 R_E near the midnight meridian plane and a thickness roughly twice this value near the boundaries with the magnetosheath (Bame et al., 1967). These average values appear to be roughly the same at distances of $\sim$ 18 R_E (Bame et al., 1967), at intermediate distances of 20-30 R_E (Hruska and Hruskova, 1970; Keath et al., 1976; Fairfield, 1979), and even near the lunar orbit at 60 R_E (Meng and Mihalov, 1972). With these dimensions the plasma sheet thickness is many times greater than the gyroradius of a typical thermal proton in the plasma sheet. (An 8 keV proton has a gyroradius of 1300 km $\simeq$ 0.2 R_E in a 10 nT field.) Contained within the plasma sheet is a current

sheet where the magnetic field reverses direction in a much thinner region that is probably several hundred to a few thousand km thick (Speiser and Ness, 1967).

The plasma sheet thickness is also known to be quite variable (Bame et al., 1967) and that the plasma sheet becomes much thinner during magnetospheric substorms (Hones et al., 1967; 1971). Just how thin is not easily determined, but 1 R_E is thought to be a likely value (e.g., Lui et al., 1975). This thinning preceeds substorm onset at distances within ~ 15 R_E (Nishida and Fujii, 1976; Pytte et al., 1976) where it is thought to be associated with the formation of an X type neutral line (Hones, 1977 and references therein). At greater distances the thinning occurs closer to the time of substorm onset and is thought to result from the tailward loss of plasma sheet field lines which have reconnected at the neutral point (e.g., Hones, 1977).

Oscillations of the current sheet contained within the plasma sheet have been identified both in the deep tail (Mihalov et al., 1970) and at closer distances (Speiser and Ness, 1967; Toichi and Miyazaki, 1976; Lui et al., 1978) by noting the quasi-periodic reversals of the tail field B_x component as the current sheet passes over the spacecraft. When these multiple crossings are observed, the current sheet reappears at time separations which may be as frequent as every few minutes. Such crossings have been attributed to a "flapping" motion of the current sheet or to wave motion in either the solar magnetospheric X (Speiser, 1979) or Y (Lui et al., 1978) directions. Toichi and Miyazaki (1976) noted that the intervals of current sheet oscillations occurred preferentially near substorm onset and in the presence of a southward interplanetary field, but they did not note that the crossings were associated with thin plasma sheets as well as thin current sheets.

The present paper uses high resolution magnetic field, thermal plasma, and energetic particle data measured on the IMP-8 spacecraft to demonstrate that a thin plasma sheet with rapidly flowing plasma undergoes violent oscillatory motion which causes the entire thickness of the plasma sheet to pass over the spacecraft in times which are sometimes as short as 10-s. Protons with 50 and 290 keV energy are investigated since their gyroradii are comparable to the plasma sheet thickness. As the spacecraft moves from the

plasma sheet into the lobe, the energetic particle intensities decrease, but the 290 keV protons are relatively more numerous than 50 kev protons on field lines located deeper in the lobe. This observation may be interpreted in terms of a neutral line model of the magnetotail where these particles are accelerated at the neutral line and the lower energies undergo relatively greater equatorward drift in a cross tail electric field. Observations of tailward streaming electrons further support this model.

INSTRUMENTATION

IMP-8 was launched on October 28, 1973 into an orbit ranging from 25-43 R_E and it traverses the magnetotail from dusk to dawn approximately every twelve days. Listed below are 4 different IMP-8 instruments used in the present study, from which data were used covering four events on three selected days.

(1) Magnetic field data from the Goddard Space Flight Center magnetometer is obtained with maximum time resolution of 25 vectors/second (Mish and Lepping, 1976). A maximum resolution of 3.1 vectors/second will be used in the present study.

(2) Thermal plasma is measured by the Los Alamos Scientific Laboratory electrostatic analyzer (Hones, 1978). Positive ions are measured in 16 logarithmically spaced energy channels from 84 ev to 15.3 keV. The instrument has a 2.5° wide acceptance fan which looks out in the spacecraft equatorial plane ± 56° and it views different azimuths as the spacecraft spins about an axis oriented perpendicular to the ecliptic. Protons are measured at 16 angles and 16 energies during five consecutive spacecraft spins of 2.6-s duration totaling 13-s. These measurements were interleaved with electron measurements and repeated every ∿26-s.

(3) The NOAA/APL energetic particle experiment measures ions and electrons at a variety of relatively high energies (Williams, 1977). Here we will use measurements of 50-220 keV ions made by a detector with an acceptance cone of 15° full width that looks perpendicular to the spacecraft spin axis. Measurements are made in 16 azimuthal angles during a single spin period. The

measurements recur every 20.4-s.

(4) The JHU/APL charged particle experiment consists of a variety of detectors which measure energetic particles moving in different directions. The experiment is essentially identical to the IMP-7 experiment described in detail by Sarris et al. (1976). Here we will use measurements of 290-500 keV protons and 220 keV ?.5 MeV electrons made by the proton-electron telescope which views a cone of 45° full width oriented perpendicular to the spin axis. Measurements are made in 8 angular sectors and they recur every 10.2 seconds. In this paper we will average successive samples of the JHU/APL data in order to match the 20.4 second time resolution of the NOAA/APL experiment, and we will average adjacent angular sectors of the NOAA data in order to match the 8 sector resolution of the APL data. In view of the rapidly decreasing particle flux with increasing energy, we will refer to each of the above proton energy ranges as 50 keV and 290 keV.

PLASMA SHEET OSCILLATIONS

Figures 1 and 2 illustrate the prevailing geomagnetic conditions, the spacecraft location and the general state of the magnetotail for the intervals discussed in this paper. The AE index is shown at the top of each figure and 15 second average values of the tail field as measured by IMP-8 are shown below. The tail field magnitude B is shown along with the B_z field component and the north-south and azimuthal angles θ and ϕ in solar magnetospheric coordinates. For the period shown in Figure 1, the interplanetary magnetic field is available from IMP-6 and the B_z component is shown below the AE panel. Spacecraft locations in solar magnetospheric coordinates are listed at the top of the figure along with the estimated distance from the equatorial current sheet, z' (Fairfield, 1980).

In Figure 1 the spacecraft is located slightly north of the current sheet (z' is positive and small and ϕ is most often near 0°). Magnetic field and plasma data (not shown) indicate that the spacecraft passed from the magnetosheath into the dusk magnetotail at ~ 1900. The intervals of interest in this study are indicated by bars over the field magnitude near 2040 and 0240. These intervals are characterized by high B, small θ and rapid reversals of ϕ

which indicate current sheet crossings. It will be demonstrated below that these times of strong B are associated with very tenuous thermal plasmas and hence these are times of plasma sheet thinning. The 0240 interval occurs near the time of an enhancement in AE whereas the 2040 interval occurs closer to the time of maximum AE. These intervals may be contrasted with the hours after 2215 and 0310 when the data indicate weak magnetic field vectors with generally large θ values and earthward flowing plasma (not shown). Such observations, which are characteristic of thick plasma sheets that typically occur as AE decreases, are often cited as evidence that a neutral line has moved tailward of an observing spacecraft during substorm recovery. Later we will discuss tailward flows which are associated with small B_z components earlier in these events.

Two similar events are seen in Figure 2 near 0650 and 0920. These events have been studied previously by Carbary and Krimigis (1979; their figures 4, 5, 8 and 9). At these times the spacecraft is located in the premidnight sector of the tail and is making a transition from the northern hemisphere (positive z' and $\phi \lesssim 0°$ at the earliest times) to the southern hemisphere (negative z' and $\phi \lesssim 180°$ at the latest times). Each of the events is associated with an enhancement of AE and reversals of ϕ. Only in the latter event were the counting rates of the thermal plasma detector large enough to allow any meaningful velocity determinations, but in this case they again indicate earthward flows associated with the large positive B_z after $\sim$ 0930. Additional plasma sheet thinnings are associated with the disturbances near 0400 and 1130 but in these cases the spacecraft was far enough north or south of the equatorial plane so that current sheet crossings were not seen. Events of the type discussed in this paper probably illustrate typical tail behavior but the spacecraft must be quite near the equatorial region (probably $z' \lesssim 0 \pm 1\ R_E$) near the time of substorms to observe the crossings. Additional examples of similar multiple current sheet crossings can be seen in Toichi and Miyazaki (1976) but these authors did not emphasize the thin plasma sheet aspects.

Detailed magnetic field data for the intervals indicated by bars in Figures 1 and 2 are shown in Figures 3-5. The same field quantities are shown as in the earlier figures only now the time resolution is one point every 320

milliseconds. The crosses superposed on the B trace indicate the magnetic field strength equivalent of the plasma pressure plus field pressure. Fairfield et al. (1981) have demonstrated that total pressure tends to be constant between the high β plasma sheet and the low β tail lobes. The approximate constancy of crosses reflects this fact although the limited energy range of the IMP-8 plasma experiment causes an underestimation of the plasma pressure, especially at times of hot plasma such as are being considered here. The 2/3 recalibration factor advocated by Fairfield et al. (1981) was not used in the present work in order to approximately compensate for the unmeasured particles above 15 keV.

It is clear that in the high field regions of Figures 3-5 little or no thermal plasma was measured. In most of the low field regions (e.g., Figure 3a, 0221; Figure 3b, 0245, 0250; Figure 4, 2043, 2051, 2047; Figure 5, 0923) the plasma compensates for the field pressure deficit although in some cases (e.g., Figure 3a, 0225; Figure 3b, 0247; Figure 5, 0907) the plasma analysis program was unable to calculate moments of the distribution function and hence no plasma pressure was obtained in spite of the fact that measured counts indicated the presence of plasma. Using these determinations of the total pressure we are able to define the average value. The magnetic field equivalent of half the total pressure $(8\pi P)^{1/2}$ is represented by the dashed lines in Figures 3-5. (A smooth dashed line is drawn to eliminate the more rapid fluctuations seen in the total pressure which are due largely to poor counting statistics for the plasma instrument over these short sampling intervals.) This dashed line can be designated the $\beta = 1$ line (β = plasma pressure/field pressure); field values above this line indicate a $\beta < 1$ plasma and field values below the line indicate a $\beta > 1$ plasma. In this paper we define the tail lobe to be a region of $\beta < 1$ plasma. Note that usually the field is well above or well below this line so the choice of $\beta <$ unity rather than, say, 0.5 is not critical.

The rectangles above the B trace in Figures 3-5 indicate the lobe regions according to the above definition. From the field polarity we can deduce whether the northern ϕ ($\approx 0°$) or the southern ($\phi \approx 180°$) tail is being measured and this is indicated by the letter above the rectangle. A primary result of the present study is the observation that rapid traversals from the

tail lobe of one hemisphere to the tail lobe of the other hemisphere occur in times as short as 10 seconds (e.g., Figure 3a, 023505; 023825; 023915; 024130; 024225: Figure 3b, 025820; Figure 4, 204825; Figure 5, 090815; 091420). In addition to these cases, Coroniti et al. (1980, Figure 8) show a single crossing that occurred in about 1 minute. During these multiple crossings the entire thickness of the plasma sheet apparently moved past the spacecraft in just these few seconds. Alternatively one could postulate a plasma sheet where low β filaments detach from the main lobe fields and such flux tubes with differing polarities intermingle within the plasma sheet. While this might be possible, the fact that the plasma sheet is already known to be quite thin at these times suggests that filamentary structure may be an unnecessarily complicated model. In the remainder of this paper we will assume the existence at a single relatively well defined, though perhaps distorted, current sheet.

In addition to the crossings of the plasma sheet noted above there are many more instances in Figures 3-5 where a transition occurs from the plasma sheet of one hemisphere to the tail lobe of the opposite hemisphere (e.g., Figure 3a, 022810; 023315; Figure 3b, 024325; 024600; 025240; 030740; Figure 5, 091130; 091230; 092110). In these cases the spacecraft has crossed at least the half thickness of the plasma sheet in a comparably short time.

In the intervals shown in Figures 3-5 plus the 0650 event in Figure 2 (not shown in detail) we find a total of 13 full crossings and 22 partial crossings. After doubling the partial crossings times we plot a histogram of these 35 crossing durations, ΔT, on the ordinate of Figure 6 which is associated with the scale at the top. Typical time durations for crossing the entire thickness of the plasma sheet are seen to be between 10 and 30 seconds.

The crossing time Δt is the only quantity directly measured by a single spacecraft, but it will be related to the apparent plasma sheet thickness T and the average sheet velocity during the crossing, V by the relation $\Delta t = T/V$. These additional parameters are also plotted in Figure 6. Without additional information we can only say that to explain the small Δt's of 10 seconds, we must have either a relatively large thickness of say $\sim$6000 km moving past the spacecraft at a high velocity of $\sim$600 km/sec or else a smaller

thickness such as ~1000 km moving at a lower velocity of ~100 km/sec. However, we appeal to additional information about crossing frequencies and oscillation amplitudes which through the following arguments indicate that the lower thicknesses and velocities are more likely.

It is common to observe plasma sheet thinnings without current sheet crossings at distances of 2 to 3 R_E from the equatorial plane (e.g., Figure 2 at ~0230 and ~1100 and Fairfield et al., 1981) so a conservative upper limit to the half amplitude, A, of the plasma sheet oscillation can be taken as 2 R_E ≈ 12000 km. The recurrence rate of the plasma sheet crossings is roughly one every 2 or 3 minutes in Figure 3 and once per minute in Figure 5. Considering that two crossings occur during every oscillation period we may take an oscillation frequency of $\omega = 2\pi/250$ sec.

One possible model for motion of the plasma sheet is shown in Figure 7a. We postulate that the sheet is moving in the z direction with its position given by $z = A \sin(\omega t)$ and its velocity by $dz/dt = A\omega \cos \omega t$. With the values for A and ω suggested above, the maximum velocity is $12000\ (2\pi/250) \approx 300$ km/sec. Considering that the amplitude estimate is an upper limit and that 300 km/sec is a maximum velocity, this estimate argues for the lower range of velocities and thicknesses in Figure 6.

Another possible model for plasma sheet oscillations postulates that waves are propagating in the tail which distort the plasma sheet and cause the crossings (Figure 7b). In this case the velocity can be interpreted as a phase velocity of the propagating waves and the frequency of crossings will be $\omega = \vec{V} \cdot \vec{k}$. In this model the plasma sheet will pass over the spacecraft at an oblique angle so that the apparent thickness T_a will be related to the actual thickness T as $T = T_a \sin\theta$. An approximate value for θ will be $\theta = \tan^{-1} 2A/\lambda$. With the above value of ω, $\lambda = 250$ V. Using this value of λ we find $\theta = \tan^{-1}$ (2x12000 km/250 V) $\approx \tan^{-1}$ (100/V). Hence even if the phase velocity of the wave is as large as 600 km/sec, θ is ~10° and the actual thickness T is only $\sin\theta = 0.16$ times the apparent thickness or ~1000 km. If the velocity is smaller the actual thickness is closer to the apparent thickness, but this is a smaller value as can be deduced from Figure 6.

ENERGETIC PARTICLES NEAR THIN PLASMA SHEETS

If plasma sheet thicknesses become as small as a few thousand kilometers as suggested in the previous section, finite gyroradius effects will become important for protons. Thermal protons of 8 keV energy will have gyroradii approaching the plasma sheet thickness and more energetic 50 and 290 keV protons with gyroradii of 3200 and 7800 km in a 10 nT field will undoubtedly have gyroradii at least as large as the sheet thickness. Gradient B drifts may be important and we must consider the character of individual particle orbits.

Several possible types of positive ion orbits are illustrated in Figure 8, which can be imagined as a view from the earth looking down the tail. Northern hemisphere field lines at the top are directed out of the page and minimum field strengths occur near the field reversal in the center. Southern hemisphere field lines in the bottom half of the figure are identical except for their reversed polarity.

Protons of orbit type A which gyrate in a field of one polarity will undergo a net dusk-dawn gradient B drift but if a detector looking in the equatorial plane is located further from this plane than the particle gyrocenter, then particles will be seen with a dawn to dusk component of velocity; this would be the situation for a spacecraft located in the lobe with the particles confined to the plasma sheet or its boundary region. Thermal particles whose energy density contributes to a pressure balance between field and plasma will predominate in the weaker fields near the field reversal. More of their gyrocenters will be located equatorward of a spacecraft near the lobe boundary and an excess of dawn to dusk moving particles will be seen. Coroniti et al. (1980) noted an absence of dawnward moving particles near the plasma sheet boundary and they argued that the 50 keV particle gradient was comparable to the gyroradius and the sheet thickness.

Protons of orbit type B cross the equatorial plane with a duskward component of velocity. They undergo a reversal in their sense of gyration as they cross the neutral sheet which causes them to move rapidly across the tail from dawn to dusk. The possibility of such "serpentine" motion has often been

discussed theoretically (e.g., Speiser, 1965; Sonnerup, 1971) but conclusive evidence for it has never been presented.

Particles with orbit type C also cross the equatorial plane but with a velocity component parallel to the plane which has the opposite sign to that which the particle has at the furthest distance from the plane. Due to the symmetry of the motion in the oppositely directed fields of the other hemisphere, the particle retraces its path and experiences no net drift as long as electric fields or other perturbations are not important. Such particles are apt to be particularly important in thin plasma sheets since they do not drift out of the sheet and since the sheet thickness may not be great enough to confine type A particle within a field of one polarity. In a thinning plasma sheet, type A particles might be converted to type C particles; in a static field configuration type C particles would not enter the plasma sheet for the same reasons they are not lost.

Azimuthal distributions of energetic ions are presented in Figures 9-11. Each panel presents count rate versus solar ecliptic longitude for a twenty second interval. The vectors in each panel indicate the azimuth of the magnetic field. The times of the various panels are indicated in Figures 3-5 by arrows at the tops of the figure. In addition to the 50 keV and the 290 keV data, the highest energy channels of the plasma experiment (11 and 15 keV) were investigated to attempt to cover a third range of gyroradii. Unfortunately these channels approach their background level as the spacecraft moves into the tail lobe and this precludes their use in the interesting boundary region where finite gyroradii effects are most important. These energies will only be shown for a few cases when their intensities were unusually high in the plasma sheet.

In Figure 9, panel a shows typical data from the plasma sheet and is representative of the several minutes prior to 0223 in Figure 3a. The peak in the distributions near 180° indicates flow down the tail and along field lines. A small displacement of the field vector and the flow to angles less than 180° is due to solar wind aberation and flaring of the tail at these locations near its dusk boundary (Fairfield, 1979). The thermal plasma experiment detected unusually high velocities approaching 1000 km/sec at this

time and hence unusually high count rates were observed in the 11 and 15 keV channels. Panel a is typical of the plasma sheet in that the shapes of the 50 and 290 keV distributions agree rather well. Sometimes one energy shows slightly higher intensities than the other, presumably due to changes in the shape of the proton energy spectrum.

Panel b shows data taken in the tail lobe 41 seconds after panel a. Now the peak in the count rate is at 90° corresponding to particles moving in the dawn to dusk direction. Presumably the small pitch angle, tailward streaming particles are located on field lines equatorward of the spacecraft and only the large pitch angle particles are detected. This distribution is similar to the four subsequent distributions taken in the tail lobe (not shown).

Panels c and d show two distributions separated by 21-s that are obtained as the spacecraft moves from the plasma sheet into the lobe near 0226. Panel c is typical of the plasma sheet. We emphasize that this agreement between the two energies is typical of most of the data because in the remainder of the paper we will concentrate on the more interesting and unusual times when the two energies exhibit different behavior. Panel d illustrates the most common way in which the two particle distributions differ from one another. The 50 keV distribution is quite similar to the tail lobe distribution seen in panel b with a peak at 90°. In contrast, the 290 keV distribution is similar to that seen 21-s earlier in the plasma sheet. A similar situation is shown in panel e for a lobe location that occurred just prior to reentry into the plasma sheet. In both these cases not only do the 290 keV particles have a higher intensity as might be expected, because of their larger gyroradii, but their distribution shows no tendency to shift toward 90° as does the 50 keV distribution. A significant number of 290 keV particles are still entering the detector with a dusk to dawn velocity component, and hence they must have gyrocenters located further into the lobe than the spacecraft. We conclude that these more energetic protons have a significantly different spatial distribution than lower energy protons with the high energy protons being relatively more numerous than lower energy ones on boundary region field lines that are deeper in the lobe.

Distributions with this characteristic difference between 290 and 50 keV

protons are rather common, but they have been observed only in the tail lobes near the plasma sheet boundaries. Their presence is indicated in Figures 3-5 by the small dot above the bars at the top of the figures. Another example of this phenomenon is shown by the successive distributions in panels f and g of Figure 9. Panel f shows a typical plasma sheet distribution, whereas panel g shows that the 50 keV particles in the lobe are depleted relative to 290 keV particles at the large angles corresponding to dawnward moving particles.

The period from 0220 to 0241 in Figure 3a is characterized by tailward flowing plasma and energetic particles. Counts in the tailward looking sector (0°) are frequently zero and they are never greater than 11 during any of the 62 sampling intervals of this period. In panel i the 50 keV count rate suddenly jumps to 554 at 0° and only 3 counts are seen at 180°. Only 21 seconds earlier a normal lobe distribution occurred (panel h) where particles of both energies are arriving from the dawnward direction. The 290 keV protons in panel i show a similar but less dramatic increase than the 50 keV protons. In the interval 20 seconds later (not shown) the 290 keV distribution becomes more similar to the intense 50 keV distribution. These earthward flowing plasmas persist until entry into the lobe near 0243. Then 90° distributions predominate until a tailward flow clearly returns at 0251. Tailward distributions continue for the remainder of the interval shown in Figure 3 except for one distribution near 0308 when the 50 keV peak of 190 counts occurs at 0°.

Distributions in Figure 10 correspond to the magnetic field plots of Figure 4. For at least an hour prior to 2035 the spacecraft has been continually immersed in a quiet high β plasma sheet. Plasma flows have been very small and the quiet character of the field has been similar to that seen from 2032-2035. Particle distributions have been similar to panel a since 2014. The primary features of these 50 keV distributions are double peaks 90° from the field direction which are even more apparent in the unaveraged 16 sector data. These distributions may indicate a population trapped on closed field lines and confined near the equatorial plane; indeed the magnetic field B_z component increased from < 1 nT to > 2 nT at $\sim$ 2012. The double peaked distributions disappear at 2035 as a more tail-like field develops with B increasing and B_z decreasing.

Four consecutive distributions taken as the spacecraft emerges from the lobe are presented in panels b-e. Intensities are low in panel b and the peaks occur at 90° as is frequently seen in the lobe. The 290 keV count rate increases in panel c but the particles are still centered at an angle less than 180° as would be expected if they are a component of a tailward flowing plasma on field lines equatorward of the spacecraft. In panel d the 290 keV fluxes increased further and show a fairly symmetric distribution relative to the field direction. In contrast the 50 kev particles are centered at an angle < 180° and hence provide another example of the characteristic difference between the distributions for the two energies. Finally, in panel e as the spacecraft moves closer to the plasma sheet the distributions are both more symmetrical relative to the field direction.

From 2038 to 2043:30 high velocity plasma flows are seen and energetic proton distributions similar to panel f are present. One unusual occurrence of this period from 2039 to 2043 is that the field direction angle ϕ is lower than its usual tail direction nearer 360°, but the particle distributions are more symmetric about the usual direction anti parallel to ~360°. Perhaps a current sheet produces a deflection of the locally measured field, whereas the particles are guided by a large scale field oriented in the more usual direction.

Panels g and h illustrate another entry into the lobe. In panel g the energetic protons are symmetric about the field direction. Only 21 seconds later the 50 keV protons are greatly diminished and peak at 90° whereas those at 290 keV are symmetric as before. In the subsequent several distributions the 50 keV protons increase slightly but remain peaked near 90° whereas the 290 keV particles have an excess at 180° and higher (i.e., panel i).

Distributions corresponding to the field plots of Figure 5 are shown in Figure 11. Panel a shows data taken seconds before one of the fastest crossings seen. This distribution also has an unusually strong peak at 90°, especially for the 50 keV protons. Since faster crossings are likely to correspond to thinner sheets, and thinner sheets correspond to type B trajectories in Figure 8, this event is a likely occurrence of such serpentine trajectories.

Another of the rare changes to earthward flow is illustrated in the consecutive distributions of panels b and c. Panel b shows a broad distribution of tailward moving particles with virtually no earthward moving particles detected in the 0° sector. Panel c taken 20 seconds later shows a dramatic increase in the earthward moving particles with 50 keV protons peaking at 237 counts. The flatish character of the distribution in panel c is probably related to the fact that a very northward field was present at this time, but the predominence of the earthward moving particles is confirmed in the following distribution (not shown) at which time the field has returned to a direction near the equatorial plane. The particles resume tailward motion within the next minute but another earthward flow episode occurs at 0921.

The development of the 0921 earthward flow interval is shown by consecutive distributions in panels d-f. In going from the lobe in panel d to the boundary region in panel e the 0° counts increase from 2 to 345 at 50 keV. The 290 keV counts do not increase significantly until the following distribution (f). These earthward flows persist until 0924 and it is interesting to observe their termination as seen in panels g-i. In g and h there appears to be evidence for a secondary maximum in the tailward (180°) direction. Suddenly in the 41-s between panels h and i the earthward moving particles completely disappear but a tailward population remains. This behavior may be related to mirroring near the earth and the effects of finite transit times (Forbes et al., 1981; Williams, 1980). An alternative explanation suggested by the rapid z motion of the plasma sheet boundary is that the detector might be sampling different field lines with different particle populations as they move past the spacecraft.

DISCUSSION AND CONCLUSIONS

One important conclusion that follows from the observation of rapid multiple crossings of the magnetotail current sheet is that a thin current sheet containing rapidly flowing plasma is highly unstable and undergoes large and rapid oscillations. Since this rapidly flowing plasma is presumably bounded by a much more tenuous and probably lower velocity plasma in the tail lobe, a velocity shear may occur and one must consider the possibility of a

Kelvin-Helmholz instability. However, examination of the condition for this instability (e.g., Boller and Stolov, 1973)

$$V^2 > (\rho_{ps}+\rho_L)(B_{ps}\cos^2\psi_{ps} + B_L\cos^2\psi_L)/4\pi\rho_{ps}\rho_L \approx (B_{ps}\cos^2\psi_{ps} + B_L\cos^2\psi_L)/4\pi\rho_L$$

indicates that this instability is unlikely. Here ρ is the density, the subscripts refer to the plasma sheet and the lobe, and ψ is the angle between the flow and the field direction. Since the right hand side of the instability condition is inversely proportional to the tenuous density in the lobe and since the flow is approximately field aligned and the cosine terms will be near unity, it will be difficult to reduce the value of the right hand side below that of the left hand side, and instability is unlikely to occur. The firehose instability offers a more attractive explanation. Theoretical work of Cowley (1978) indicates that thin current sheets are expected to be associated with $p_{\parallel} > p_{\perp}$ and the occurrence of this instability. The importance of this instability is speculative, but it is supported by some evidence of field aligned low energy electrons.

We note that the highly variable B_z in Figures 3-5 that occurs during these intervals of instability is consistent with the results of Caan et al. (1979) who compared the direction of B_z to the plasma flow direction in an attempt to test the theory of neutral line formation. They found significantly more southward B_z associated with tailward flow than with earthward flow as predicted by reconnection theory, but still northward fields intermingled with southward fields with the former occurring slightly more frequently. Perhaps oscillations associated with an unstable current sheet produce substantial northward and southward components from a field that would otherwise have small B_z. It is also interesting to notice the occurrence of negative-positive oscillations in B_z at several current sheet crossings (e.g., 0239 and 0241 in Figure 3a) that are similar to the signature of "flux transfer events" identified by Russell and Elphic (1979) at the dayside magnetopause.

A second important conclusion of the present paper follows from the identification of the high β plasma sheet and the observation of its rapid and repetitive movements across the spacecraft. The plasma sheet must be very

thin and/or rapidly moving, and we have argued that at these particular times the plasma sheet thicknesses do not exceed a few thousand km. Historically the plasma sheet has been identified simply by the presence of plasma (or even a particular component of the plasma such as > 40 keV electrons) above a detector threshold. It has been implicitly understood that β in the plasma sheet is generally greater than unity. Recently results from more sensitive instruments on the ISEE spacecraft (e.g., Sharp et al., 1980; Parks et al., 1979; Mobius et al., 1980; Spjeldvik and Fritz, 1981) are finding interesting phenomena which occur in more tenuous $\beta < 1$, "boundary layer" plasmas which are located between the lobe and the $\beta > 1$ plasma sheet. We emphasize that the plasma sheet that becomes thin in the present paper is that defined by $\beta > 1$, and hence it corresponds more closely to the traditional plasma sheet. The energetic particles seen adjacent to it may be considered to be part of the boundary layers.

A third major conclusion follows from the behavior of energetic particles near the plasma sheet boundary. Particles with gyrocenters near the high latitude boundary of the plasma sheet are expected to penetrate half a gyroradius into the lobe; as the spacecraft moves into the lobe the lower energies with smaller gyroradii might be expected to disappear before the higher energies provided that various energies have similar density gradients near the boundary. In fact, this type of energy dependence was seldom seen. The peak of the azimuthal distribution often moved from field-aligned (180°) to duskward moving (90°) as the spacecraft moved into the lobe, and this is indeed consistent with expected particle gradients and larger populations of particles with gyrocenters nearer the plasma sheet. The significant and surprising result is the frequent and consistent difference between 50 and 290 keV particles; the higher energy particles remaining symmetric about the field direction after the peak in 50 keV particles moves to 90°. At these times there are as many 290 keV particles with gyrocenters further into the lobe as there are with gyrocenters closer to the plasma sheet. This situation (the dots above the bars in Figures 3-5) occurs regardless of whether the spacecraft is entering or exiting the plasma sheet.

To explain the above observations, we see no alternative other than to postulate an energy-dependent spatial distribution of particles with the

higher energies being relatively more numerous on flux tubes contained deeper in the lobe. To create this situation we invoke the explanation proposed by Sarris and Axford (1979) whereby particles are energized at an earthward location such as a neutral line and launched tailward on flux tubes near the plasma sheet boundary. These particles move in the presence of a cross tail electric field and they drift toward the equatorial plane. The slower, less energetic particles have more time to drift toward the equatorial plane than the more energetic ones which are, therefore, preferentially seen on field lines closer to the lobe.

To further investigate the possibility of acceleration at a neutral line, we have investigated the angular distribution of energetic electrons. Previous observations (Bieber and Stone, 1980 and references therein) have detected tailward streaming electrons (E_e > 200 keV) associated with both substorms and southward tail magnetic field components. These observations have been interpreted as evidence for neutral line acceleration of the electrons and their subsequent tailward propagation on newly created open field lines. Indeed, we find evidence for tailward streaming electrons in the E_e > 220 keV channel of the JHU/APL experiment. Earthward streaming is not seen. The presence of such streaming is indicated in Figures 3-5 by the presence of triangles at the bottom of the B_z panels.

The longest interval of streaming electrons occurs in Figure 5 from 0901-0904. It is associated with southward B_z and follows immediately after an interval of even more southward B_z (see Figure 2) in the manner described by Bieber and Stone (1980). Both this interval and most of the shorter duration intervals of tailward streaming in Figures 3-5 are seen to occur on lobe field lines rather than within the plasma sheet, but especially at locations near the lobe-plasma sheet transition. Although this location for streaming electrons has not been discussed in previous studies, which have generally been constructed with lower resolution magnetic field data, it seems to be very consistent with the neutral line acceleration model as described above.

The description of energetic ion populations described above is based on distributions which are frequently and consistently seen on field lines near

the plasma sheet boundary. It involves a spatial distribution of particles that is essentially constant relative to the plasma sheet boundary and this distribution moves back and forth across the spacecraft. Williams (1981) has recently explained ISEE observations of energetic protons observed near the plasma sheet boundary with a fundamentally different explanation. He argues that complex energy and pitch angle dependences are easily explained by a time-dependent particle source that sporadically emits particles along flux tubes connected to the spacecraft. Although this is a fundamentally different explanation, we feel that it is quite possible that both of these alternatives are relevant at different times.

In support of this position where both spatial and temporal changes may be important, we note the following. In the work of the present paper the characteristic differences between the two energies are not always observed and this implies that there is some time dependence in our basically static picture. In addition, explicit time dependence of electrons and ions are also seen; intensity variations are not entirely due to motion from a low intensity region to a high intensity region because sometimes the spacecraft can be clearly immersed in the plasma sheet or the tail lobe and suddenly particles of different energies increase dramatically. At other times, such as 0241 in Figures 3a and 9 and 0921 in Figures 5 and 11 ion flow reversals suddenly occur to directions not previously seen, although the earlier arrival of lower energy particles is difficult to explain even with Williams' picture. The persistence of 180° particles in Figure 11i after the termination of earthward moving particles (11h) is completely consistent with Williams' explanation. While emphasizing the spatial aspect of the particles to explain one result we certainly do not exclude the occurrence of time variations.

Other differences between Williams' boundary particles and those discussed in this paper should be emphasized. Although Williams locates his events near the plasma sheet boundary by noting their proximity to regions of intense 24-44 keV particles thought to be characteristic of the plasma sheet, it is clear from the minimal variation in his magnetic field data that the spacecraft does not enter the high β plasma sheet. Also his events are located well away from the equatorial region and certainly do not correspond to thin plasma sheets.

Acknowledgments

The authors express appreciation to the principle investigator on the NOAA/APL energetic particle experiment, D. J. Williams, for supplying the 50 keV ion data and helpful comments. Instrumental in supplying additional data were our immediate colleagues R. P. Lepping and N. F. Ness (magnetic field), S. J. Bame and J. R. Asbridge (plasma) and S. M. Krimigis (energetic particles). Numerous people supplied helpful comments on early versions of the manuscript. C.I.M. acknowledges support of NSF Atmospheric Sciences division grant ATM-7923240 to the Johns Hopkins University Applied Physics Laboratory.

REFERENCES

Bame, S. J., J. R. Asbridge, H. E. Felthauser, E. W. Hones, and I. B. Strong, Characteristics of the plasma sheet in the earth's magnetotail, J. Geophys. Res., 72, 113, 1967.

Bieber, J. W., and E. C. Stone, Streaming energetic electrons in earth's magnetotail: Evidence for substorm associated magnetic reconnection, Geophys. Res. Lett., 7, 945-948, 1980.

Boller, B. R., and H. L. Stolov, Explorer 18 study of the stability of the magnetopause using a Kelvin-Helmholtz instability criterion, J. Geophys. Res., 78, 8078-8086, 1973.

Caan, M. N., R. H. Fairfield and E. W. Hones, Jr., Magnetic fields in flowing magnetotail plasmas and their significance for magnetic reconnection, J. Geophys. Res., 84, 1971, 1979.

Carbary, J. F., and S. M. Krimigis, Energetic particle activity at 5-min and 10-s time resolution in the magnetotail and its relation to auroral activity, J. Geophys. Res., 84, 7123, 1979.

Coroniti, F. V., L. A. Frank, D. J. Williams, R. P. Lepping, F. L. Scarf, S. M. Krimigis and G. Gloeckler, Variability of plasma sheet dynamics, J. Geophys. Res., 85, 2957, 1980.

Cowley, S. W. H., The effects of pressure anisotropy on the equilibrium structure of magnetic current sheets, Planet. Space Sci., 26, 1037, 1978.

Fairfield, D. H., On the average configuration of the geomagnetic tail, J. Geophys. Res., 84, 1950, 1979.

Fairfield, D. H., A statistical determination of the shape and position of the geomagnetic neutral sheet, J. Geophys. Res., 85, 775, 1980.

Fairfield, D. H., R. P. Lepping, E. W. Hones, Jr., S. J. Bame, and J. R.

Asbridge, Simultaneous measurements of magnetotail dynamics by Imp spacecraft, J. Geophys. Res., 86, 1396, 1981.

Forbes, T. G., E. W. Hones, S. J. Bame, J. R. Asbridge, G. Paschmann, N. Sckopke, and C. T. Russell, Evidence for the tailward retreat of a magnetic neutral line in the magnetotail during substorm recovery, Geophys. Res. Lett., 8, 261, 1981.

Hones, E. W., Jr., Substorm processes in the magnetotail: Comments on 'On hot tenuous plasmas, fireballs, and boundary layers in the earth's magnetotail' by L. A. Frank, K. L. Ackerson and R. P. Lepping, J. Geophys. Res., 82, 5633, 1977.

Hones, E. W., Jr., Some characteristics of rapidly flowing magnetotail plasmas: Further comments on 'On hot tenuous plasmas, fireballs, and boundary layers in the earth's magnetotail' by L. A. Frank, K. L. Ackerson, and R. P. Lepping, J. Geophys. Res., 83, 3358, 1978.

Hones, E. W., Jr., J. R. Asbridge, S. J. Bame, and I. B. Strong, Outward flow of plasma in the magnetotail following geomagnetic bays, J. Geophys. Res., 72, 5879, 1967.

Hones, E. W., Jr., J. R. Asbridge, and S. J. Bame, Time variations of the magnetotail plasma sheet at 18 R_E determined from concurrent measurements by a pair of Vala satellites, J. Geophys. Res., 76, 4402, 1971.

Hruska, A., and J. Hruskova, Transverse structure of the earth's magnetotail and fluctuations of the tail magnetic field, J. Geophys. Res., 75, 2449, 1970.

Keath, E. P., E. C. Roelof, C. O. Bostrom, and D. J. Williams, Fluxes of $\geq$ 50 keV protons and $\geq$ 30 keV electrons at $\sim$35 R_E: 2. Morphology and flow patterns in the magnetotail, J. Geophys. Res., 81, 2315, 1976.

Lui, A. T. Y., E. W. Hones, Jr., D. Venkatesan, S.-I. Akasofu and S. J. Bame, Complete plasma dropouts at Vela satellites during thinning of the plasma

sheet, J. Geophys. Res., 80, 4649, 1975.

Lui, A. T. Y., C.-I. Meng, and S.-I. Akasofu, Wavy nature of the magnetotail neutral sheet, Geophys. Res. Lett., 5, 279, 1978.

Meng, C.-I., and J. D. Mihalov, On the diamagnetic effect of the plasma sheet near 60 R_E, J. Geophys. Res., 77, 4661, 1972.

Mihalov, J. D., D. S. Colburn and C. P. Sonet, Observations of magnetopause geometry and waves at the lunar distance, Planet. Space Sci., 18, 239, 1970.

Mish, W. H., and R. P. Lepping, Magnetic field experiment data processing systems: Explorers 47 and 50, GSFC X-694-76-158, Greenbelt, MD, August 1976.

Mobius, E., F. M. Ipavich, M. Scholer, G. Gloeckler, D. Hovestadt, and B. Klecker, Observations of a non-thermal ion layer at the plasma sheet boundary during substorm recovery, J. Geophys. Res., 85, 5143, 1980.

Nishida, A., and K. Fujii, Thinning of the near-earth (10 ~ 15 R_E) plasma sheet preceeding the substorm expansion phase, Planet. Space Sci., 24, 849, 1976.

Parks, G. K., C. J. Lin, K. A. Anderson, R. P. Lin and H. Reme, ISEE 1 and 2 particle observations of outer plasma sheet boundary, J. Geophys. Res., 84, 6471, 1979.

Pytte, T., R. L. McPherron, M. G. Kivelson, H. I. West, Jr., and E. W. Hones, Jr., Multiple-satellite studies of magnetospheric substorms: Radial dynamics of the plasma sheet, J. Geophys. Res., 81, 5921, 1976.

Russell, C. T., and R. C. Elphic, ISEE observations of flux transfer events at the dayside magnetopause, Geophys. Res. Lett., 6, 33, 1979.

Sarris, E. T., and W. I. Axford, Energetic protons near the plasma sheet

boundary, Nature, 277, 460, 1979.

Sarris, E. T., S. M. Krimigis, and T. P. Armstrong, Observations of magnetospheric bursts of high-energy protons and electrons at ~35 R_E with Imp 7, J. Geophys. Res., 81, 2341, 1976.

Sharp, R. D., D. L. Carr, W. K. Peterson, and E. G. Shelley, Ion streams in the magnetotail, preprint, 1980.

Sonnerup, B. U. O., Adiabatic orbits in a magnetic null sheet, J. Geophys. Res., 76, 8211, 1971.

Spjeldvik, W. N. and T. A. Fritz, Energetic ion and electron observations of the geomagnetic plasma sheet boundary layer: Three dimensional results from ISEE-1, J. Geophys. Res., 86, 2480-2486, 1981.

Speiser, T. W., Particle trajectories in model current sheets, J. Geophys. Res., 70, 4219, 1965.

Speiser, T. W. and N. F. Ness, The neutral sheet in the geomagnetic tail: Its motion, equivalent currents, and field line reconnection through it, J. Geophys. Res., 72, 131, 1967.

Toichi, Tsutomu, and Teruki Miyazaki, Flapping motions of the tail plasma sheet induced by the interplanetary magnetic field variations, Planet. Space Sci., 24, 147, 1976.

Williams, D. J., The ion-electron magnetic separation and solid state detector system flow on Imp 7 and 8: $E_p \geq 50$ keV, $e_e \geq 30$ keV, NOAA Technical Report ERL 393-SEL 40, 1977.

Williams, D. J., Energetic ion beams at the edge of the plasma sheet, ISEE 1 observations plus a simple explanatory model, preprint, 1980.

FIGURE CAPTIONS

Figure 1. Magnetotail magnetic field magnitude data on April 29-30, 1974 plotted along with the auroral zone magnetic activity index AE and the B_z component of the interplanetary magnetic field. The solar magnetospheric coordinates of the spacecraft are listed at the top of the figure along with the estimated distance of the spacecraft from the neutral sheet, z'. The bars above the B trace indicate the intervals of multiple current sheet crossings presented in detail in Figures 3 and 4.

Figure 2. Data for September 11, 1975 displayed in a similar format to Figure 1. Bars above the B trace indicate intervals studied in detail. The 0920 interval is presented in detail in Figure 5.

Figure 3. Magnetic field magnitude B and solar magnetospheric latitude and azimuthal angles θ and ϕ along with the B_z component are plotted at a time resolution of 320 ms. Rectangles at the top of the figure designate intervals of strong tail lobe magnetic field with the polarity of the northern or southern hemisphere indicated by n or s. Arrows indicate the times of proton angular distributions presented in Figure 9. Dots indicate times when the two particle distributions indicate an excess of higher energy protons further from the current sheet. Triangles above the time line indicate times of tailward streaming electrons. One of the fastest plasma sheet crossings occurs at 0230:20.

Figure 4. High resolution for April 29, 1974 presented in the same format as Figure 3.

Figure 5. High resolution data for September 11, 1975 presented in the same format as Figure 3.

Figure 6. A histogram of plasma sheet crossing time durations shown on the vertical axis uses the scale at the top of the figure. Appropriate plasma sheet thicknesses, T, and velocities necessary to explain the observed time durations can be read from the figure.

Figure 7. Two simple models of plasma sheet motion that could explain the observed plasma sheet oscillations (see text).

Figure 8. Illustrating the V_y and V_z motion for three classes of particle trajectories in a simple tail field model with $\vec{B} = B_x$.

Figure 9. Illustrating angular distributions of protons of various energies. Tailward moving particles are seen near 180°, earthward moving particles at 0° and duskward moving particles at 90°. The arrows indicate the measured magnetic field direction.

Figure 10. Angular distributions for April 29, 1974 in the same format as Figure 9.

Figure 11. Angular distributions for September 11, 1975 in the same format as Figure 9.

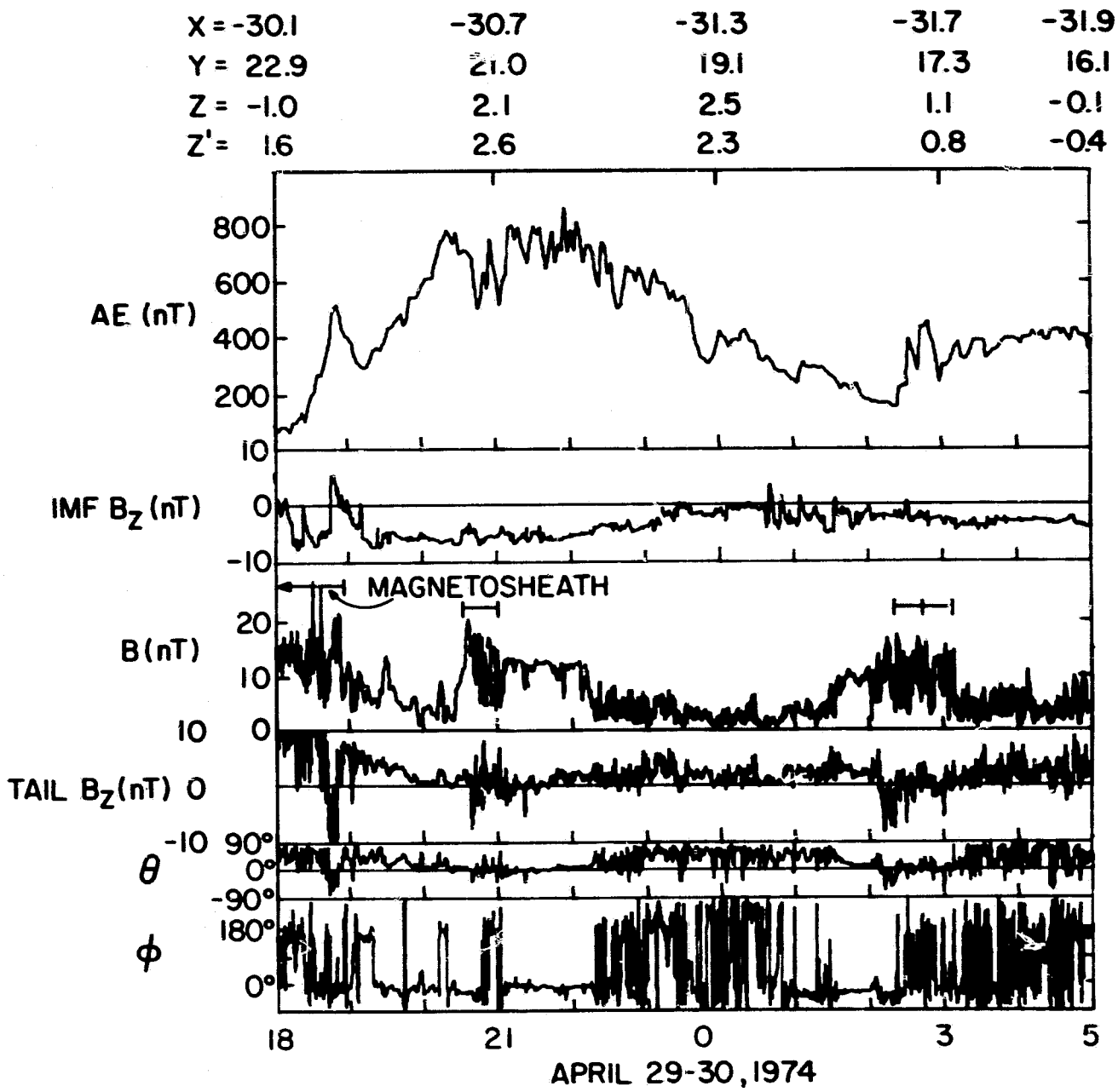

Figure 1

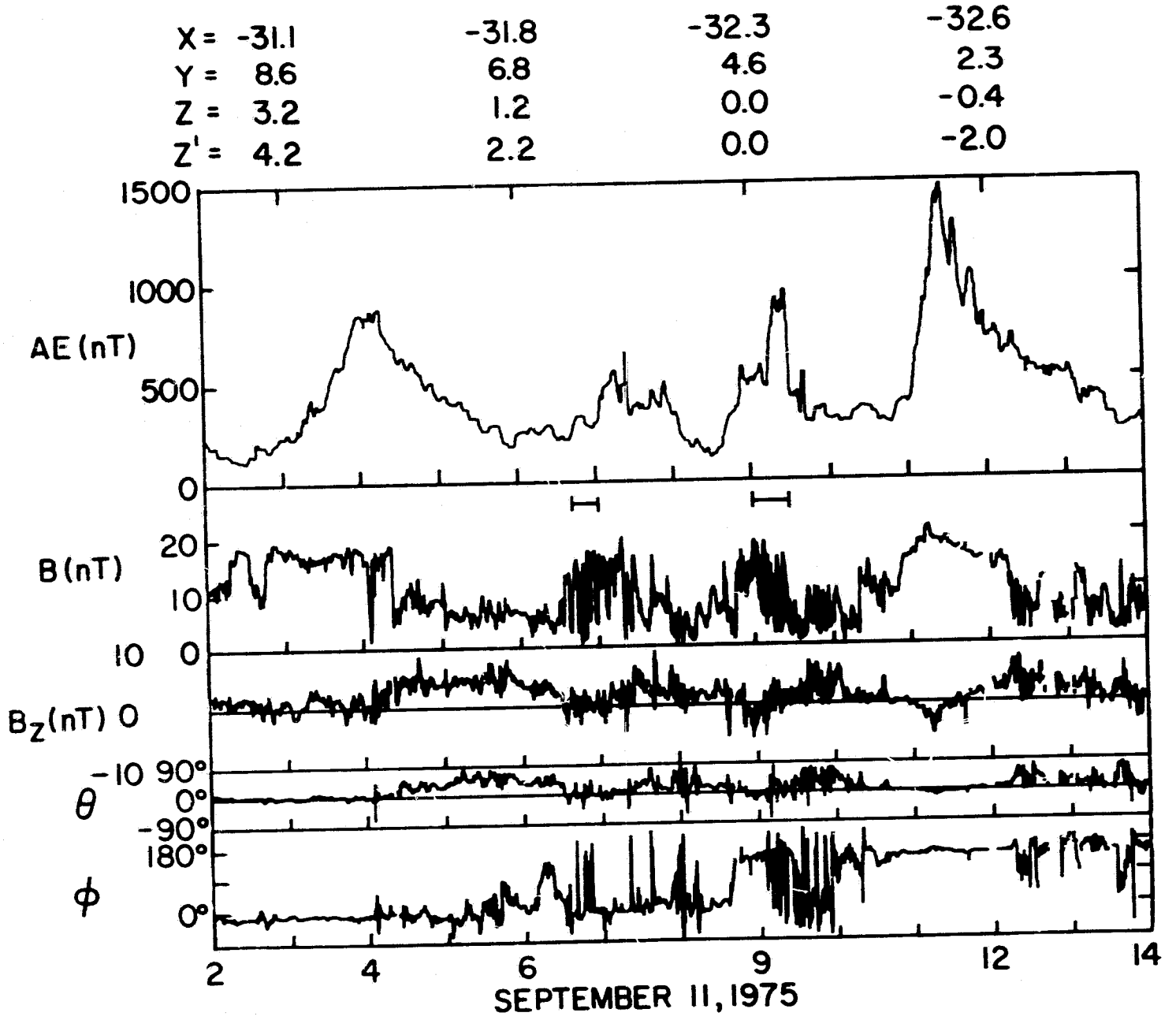
X = -31.1
-31.8
-32.3
-32.6
Y = 8.6
6.8
4.6
2.3
Z = 3.2
1.2
0.0
-0.4
Z' = 4.2
2.2
0.0
-2.0
1500
1000
500
0
AE (nT)
20
10
0
B (nT)
10
0
-10
B_Z (nT) 0
90°
0°
-90°
θ
180°
0°
φ
2
4
6
9
12
14
SEPTEMBER 11, 1975

Figure 2

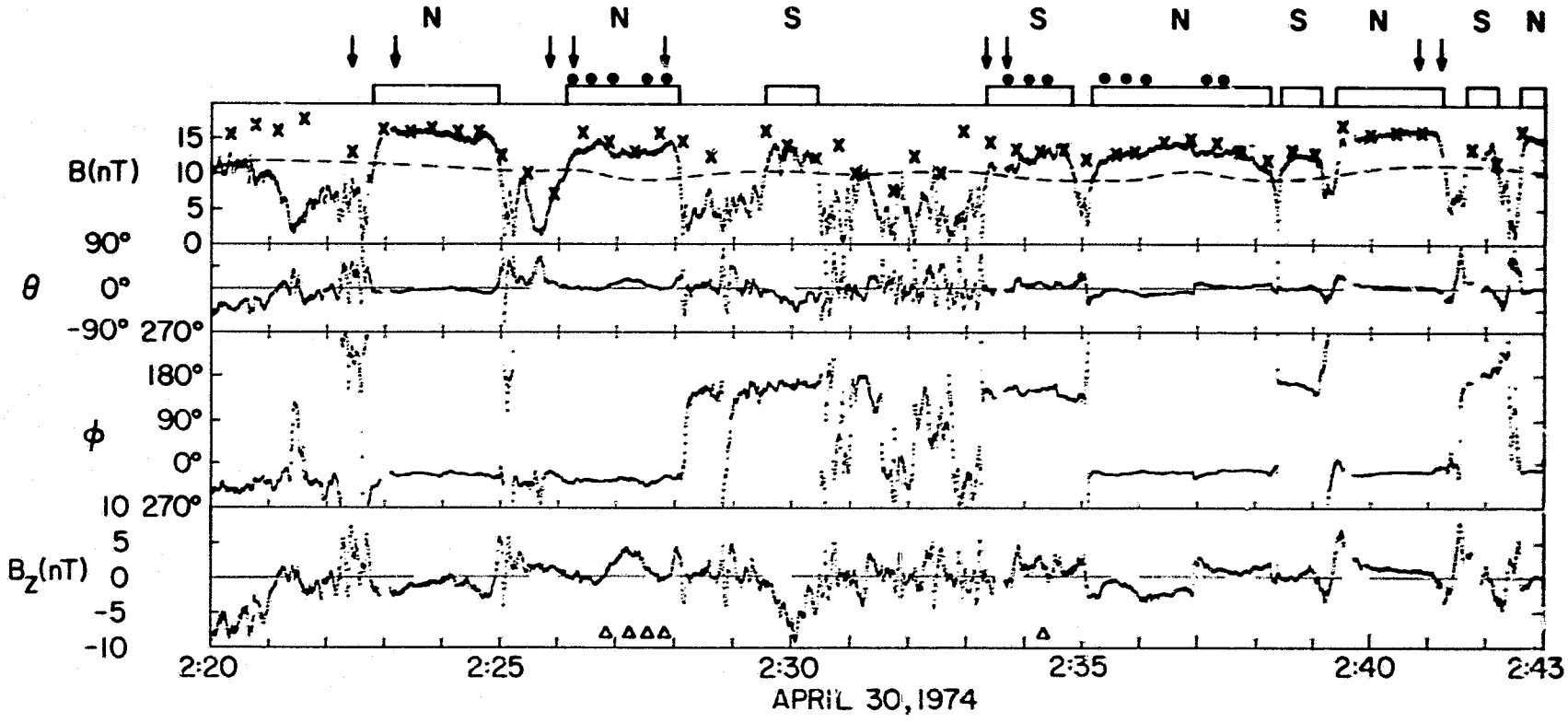
N
N
S
S
N
S
N
S
N
B(nT)
15
10
5
0
90°
θ
0°
-90°
270°
180°
90°
φ
0°
10
270°
5
0
-5
-10
B_Z(nT)
2:20
2:25
2:30
2:35
2:40
2:43
APRIL 30, 1974

Figure 3a

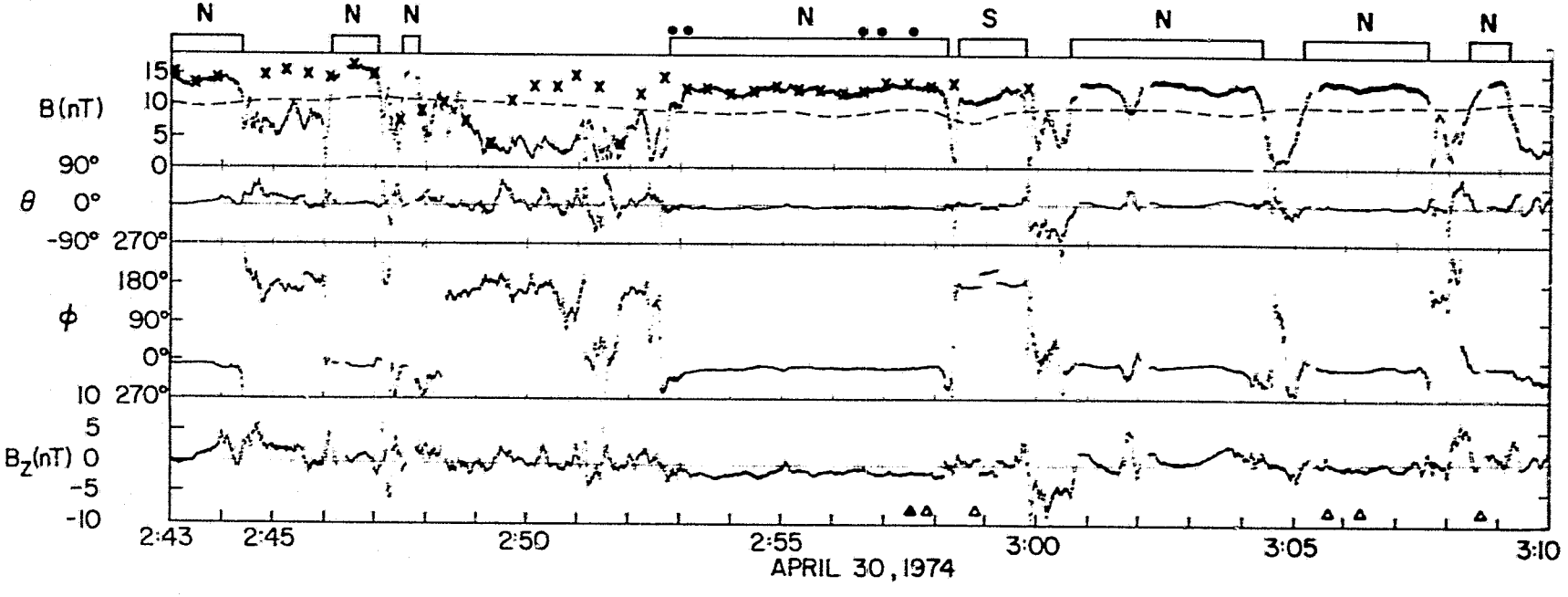
N
N
N
N
S
N
N
N
B(nT)
15
10
5
0
90°
θ 0°
-90° 270°
180°
φ 90°
0°
10 270°
5
B_Z(nT) 0
-5
-10
2:43
2:45
2:50
2:55
3:00
3:05
3:10
APRIL 30, 1974

Figure 3b

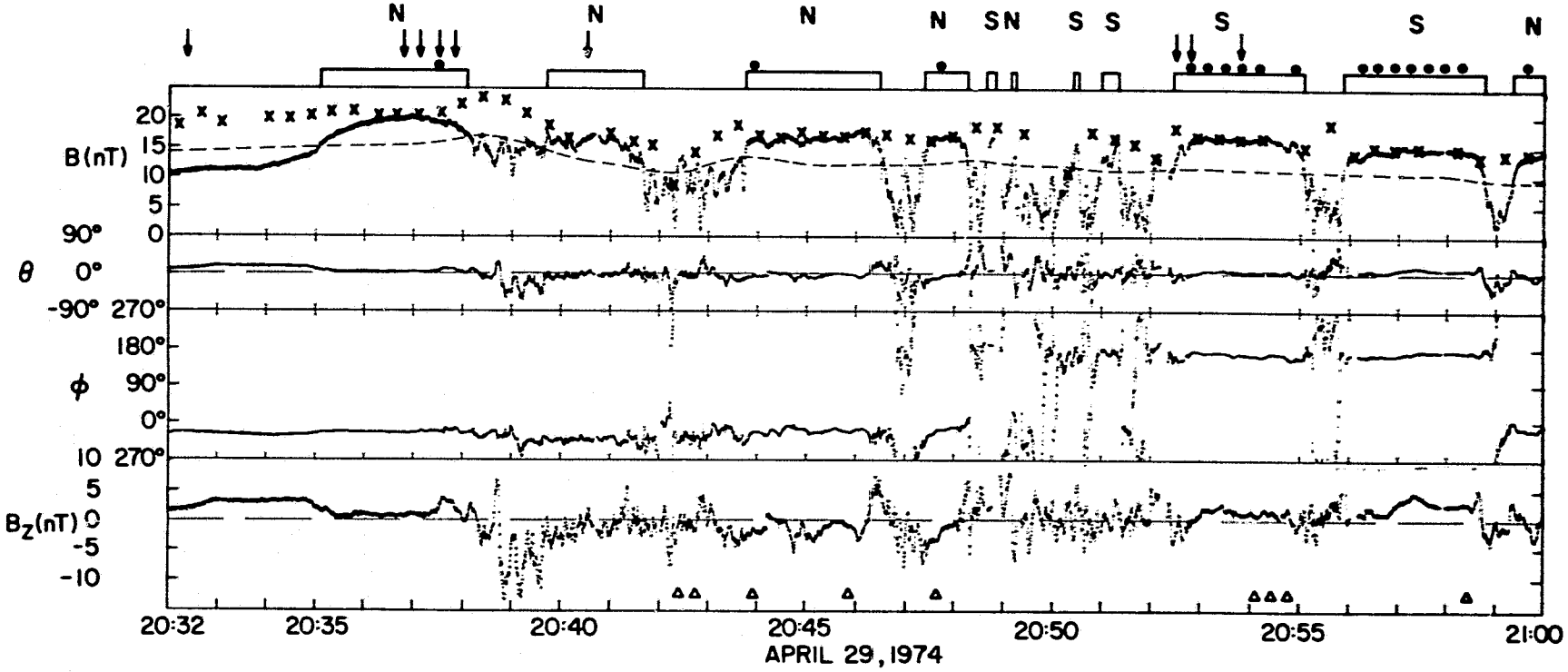
N
N
N
N
SN
S
S
S
S
N
B(nT)
20
15
10
5
0
90°
θ
0°
-90°
270°
180°
φ
90°
0°
10
270°
5
B_Z(nT) 0
-5
-10
20:32
20:35
20:40
20:45
20:50
20:55
21:00
APRIL 29, 1974

Figure 4

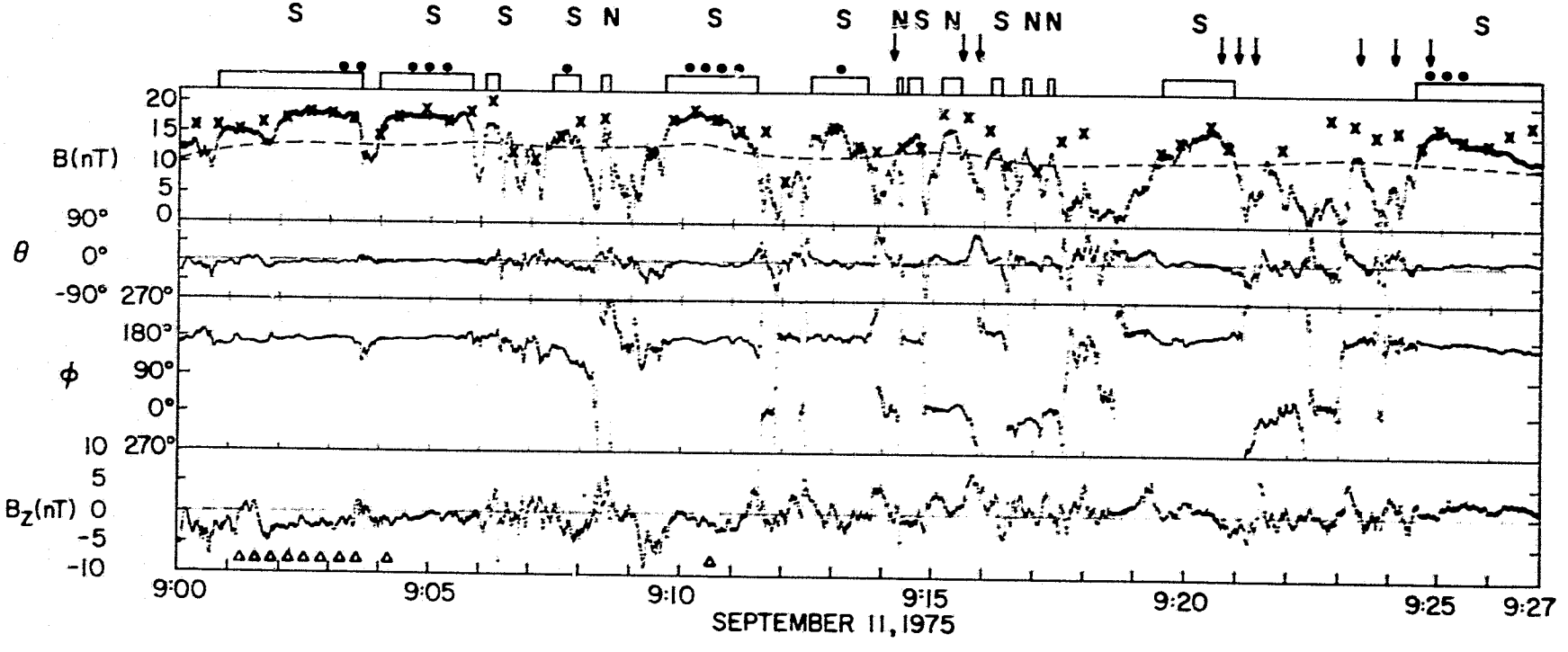
S S S S N S S N S N S N N S S
B(nT)
20
15
10
5
0
90°
θ 0°
-90° 270°
180°
φ 90°
0°
10 270°
5
B_Z(nT) 0
-5
-10
9:00
9:05
9:10
9:15
9:20
9:25
9:27
SEPTEMBER 11, 1975

Figure 5

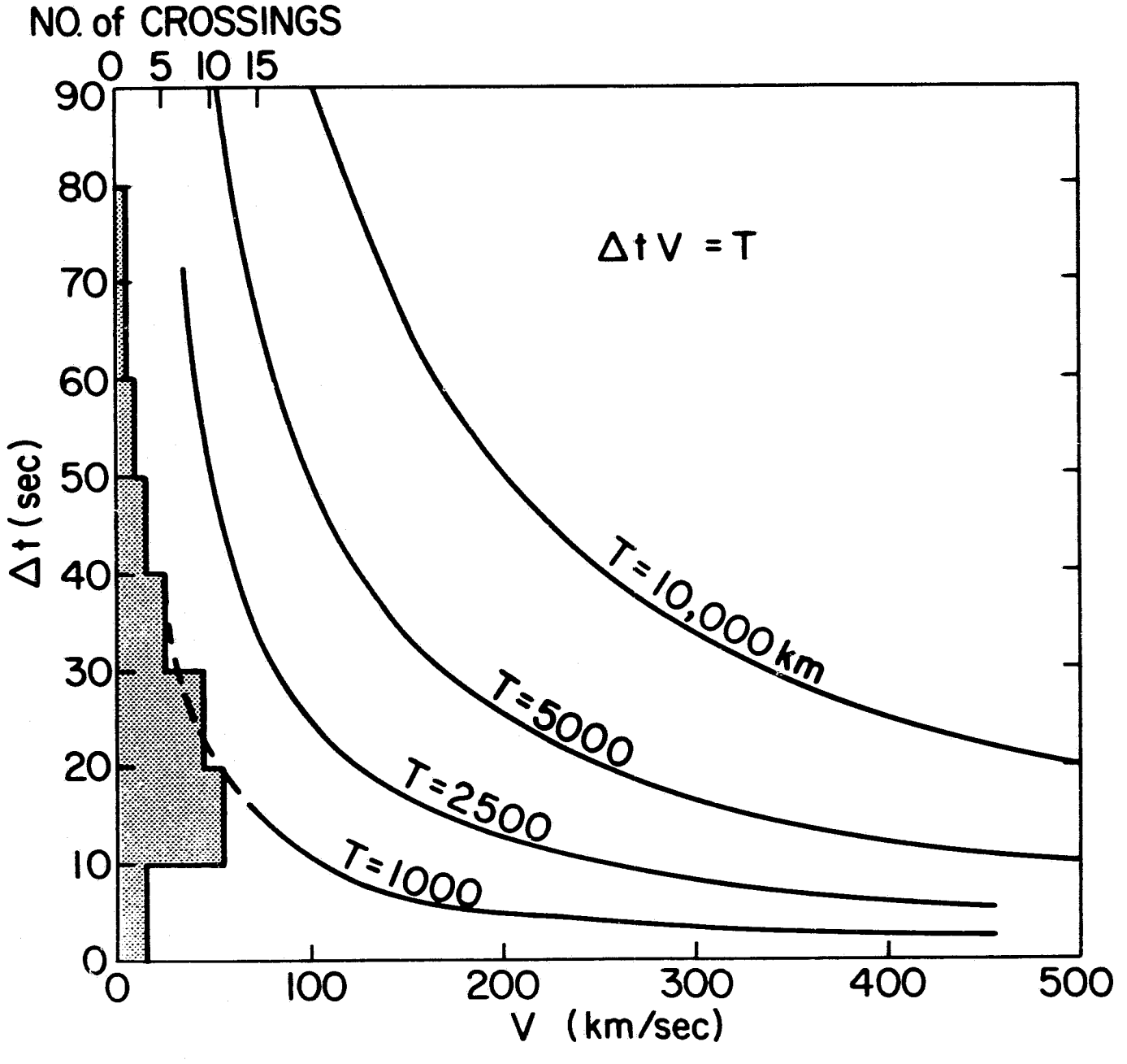
NO. of CROSSINGS
0 5 10 15
90
80
70
60
50
40
30
20
10
0
Δt (sec)
ΔtV = T
T=10,000 km
T=5000
T=2500
T=1000
0
100
200
300
400
500
V (km/sec)

Figure 6

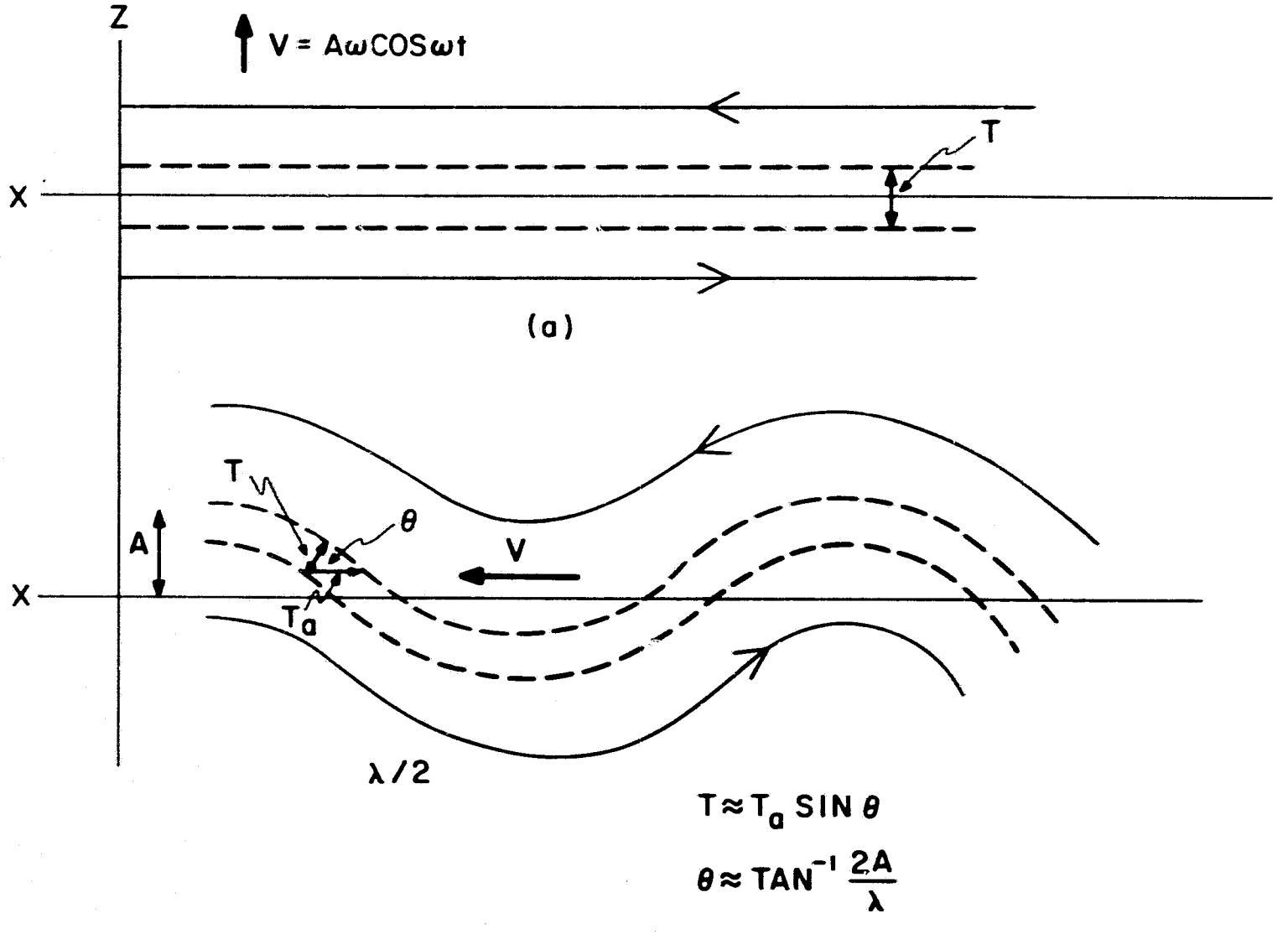

Figure 7

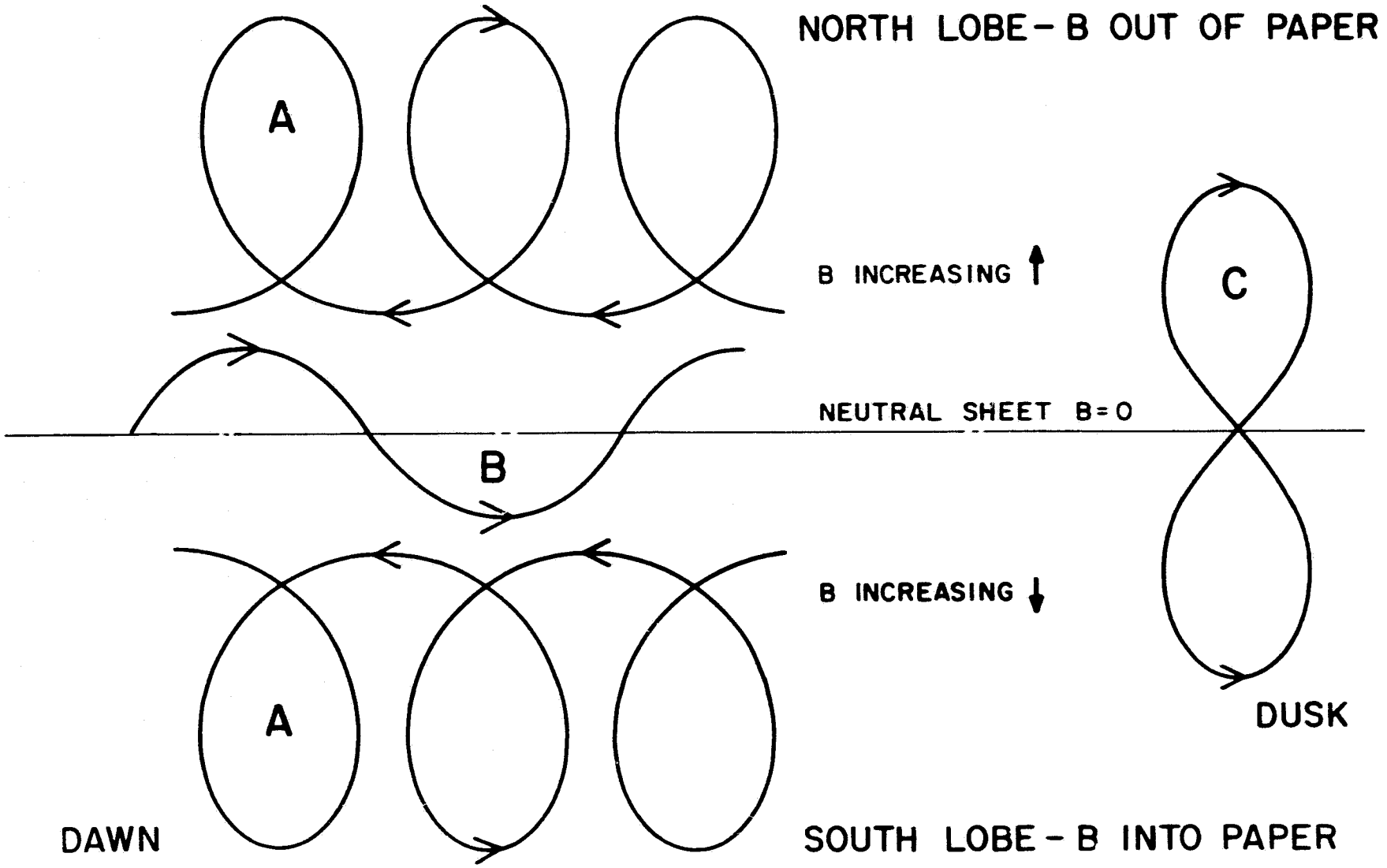
NORTH LOBE - B OUT OF PAPER
A
B INCREASING
C
NEUTRAL SHEET B = 0
B
B INCREASING
A
DUSK
DAWN
SOUTH LOBE - B INTO PAPER

Figure 8

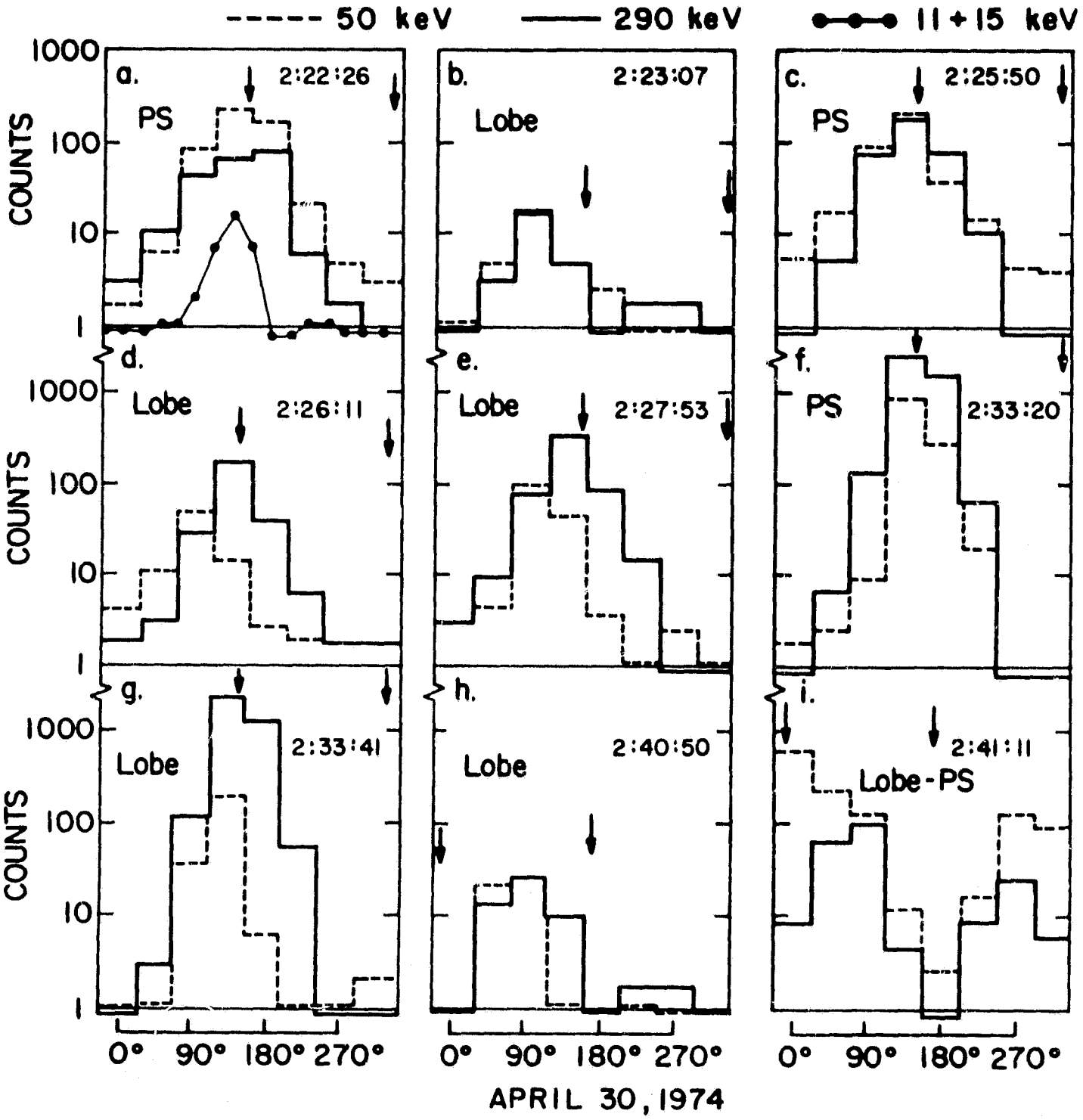
50 keV
290 keV
11+15 keV
a.
2:22:26
PS
b.
2:23:07
Lobe
c.
2:25:50
PS
d.
Lobe
2:26:11
e.
Lobe
2:27:53
f.
PS
2:33:20
g.
Lobe
2:33:41
h.
Lobe
2:40:50
i.
2:41:11
Lobe-PS
COUNTS
1000
100
10
1
0°
90°
180°
270°
APRIL 30, 1974

Figure 9

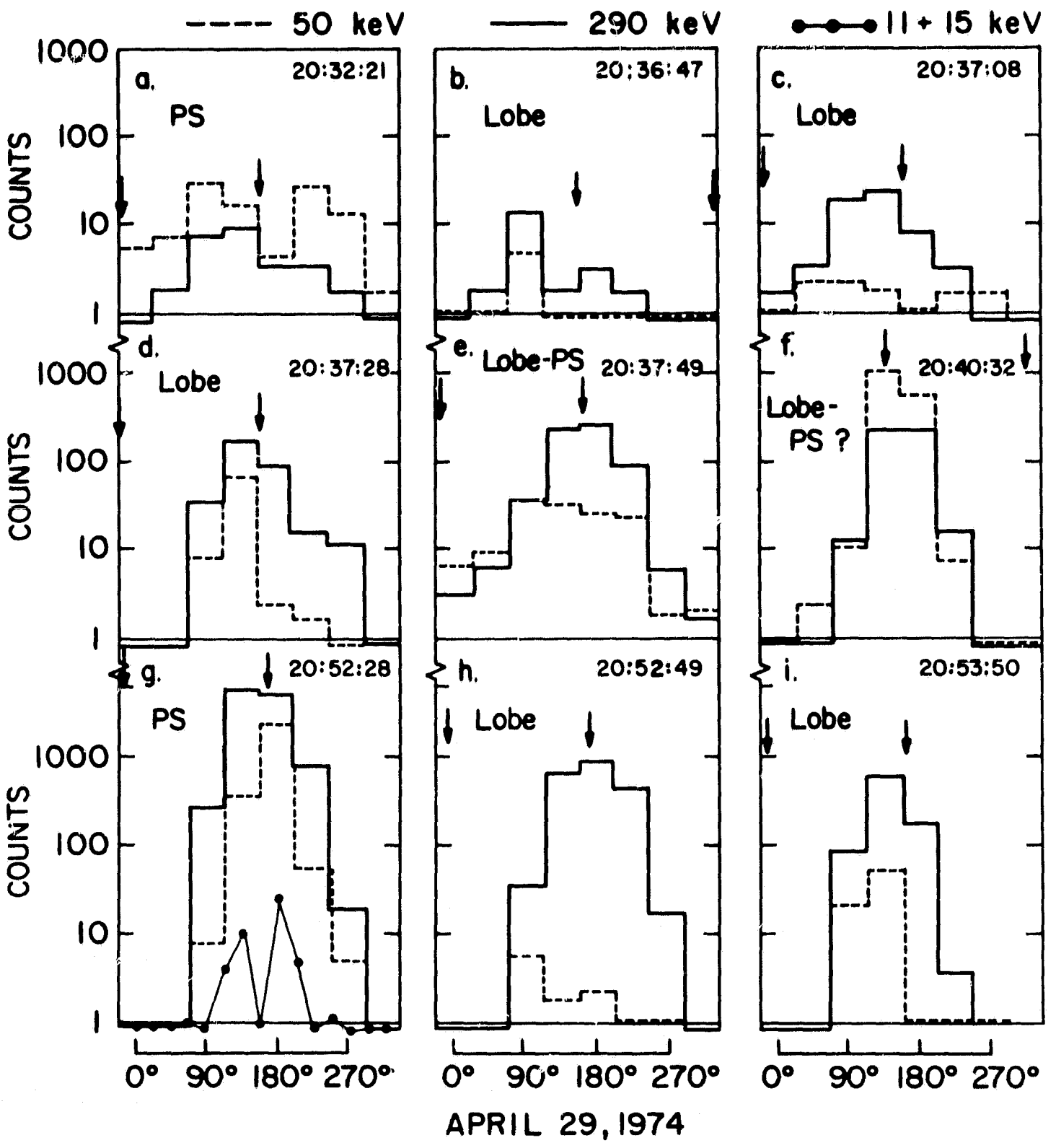
50 keV
290 keV
11 + 15 keV
COUNTS
1000
100
10
1
a.
20:32:21
PS
b.
20:36:47
Lobe
c.
20:37:08
Lobe
d.
20:37:28
Lobe
e.
Lobe-PS
20:37:49
f.
20:40:32
Lobe-
PS ?
g.
20:52:28
PS
h.
20:52:49
Lobe
i.
20:53:50
Lobe
0° 90° 180° 270°
APRIL 29, 1974

Figure 10

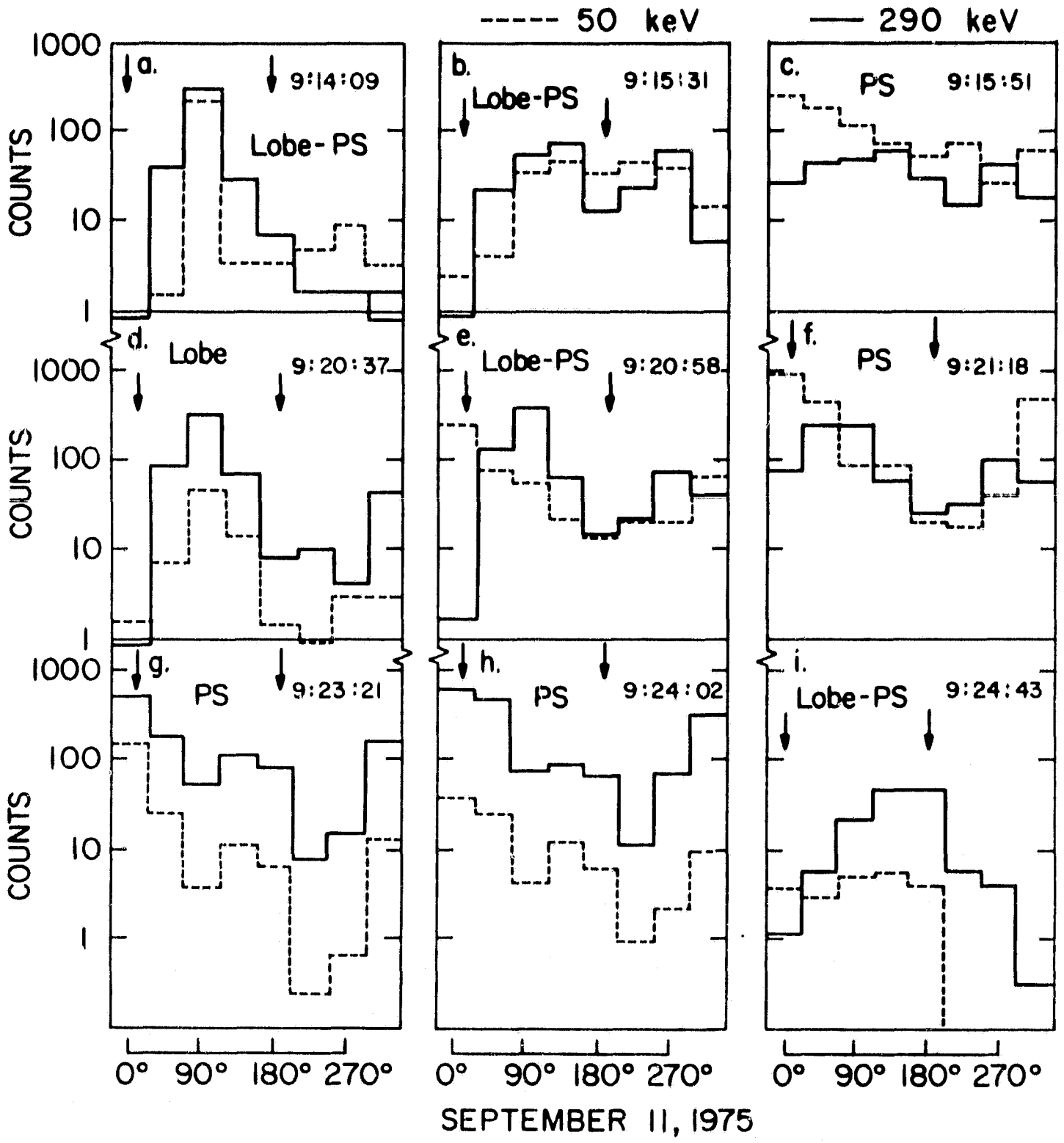
----- 50 keV
—— 290 keV
COUNTS
1000
100
10
1
a.
9:14:09
Lobe-PS
b.
Lobe-PS
9:15:31
c.
PS
9:15:51
d.
Lobe
9:20:37
e.
Lobe-PS
9:20:58
f.
PS
9:21:18
g.
PS
9:23:21
h.
PS
9:24:02
i.
Lobe-PS
9:24:43
0° 90° 180° 270°
SEPTEMBER 11, 1975

Figure 11